Development 136, 2165-2175 (2009) doi:10.1242/dev.033563

ojoplano-mediated basal constriction is essential for optic cup morphogenesis

Juan Ramon Martinez-Morales[1,2,*], Martina Rembold[1], Klaus Greger[3], Jeremy C. Simpson[3], Katherine E. Brown[1], Rebecca Quiring[1], Rainer Pepperkok[3], Maria D. Martin-Bermudo[2], Heinz Himmelbauer[4,†] and Joachim Wittbrodt[1,*,‡]

Although the vertebrate retina is a well-studied paradigm for organogenesis, the morphogenetic mechanisms that carve the architecture of the vertebrate optic cup remain largely unknown. Understanding how the hemispheric shape of an eye is formed requires addressing the fundamental problem of how individual cell behaviour is coordinated to direct epithelial morphogenesis. Here, we analyze the role of *ojoplano* (*opo*), an uncharacterized gene whose human ortholog is associated with orofacial clefting syndrome, in the morphogenesis of epithelial tissues. Most notably, when *opo* is mutated in medaka fish, optic cup folding is impaired. We characterize optic cup morphogenesis in vivo and determine at the cellular level how *opo* affects this process. *opo* encodes a developmentally regulated transmembrane protein that localizes to compartments of the secretory pathway and to basal end-feet of the neuroepithelial precursors. We show that Opo regulates the polarized localization of focal adhesion components to the basal cell surface. Furthermore, tissue-specific interference with integrin-adhesive function impairs optic cup folding, resembling the ocular phenotype observed in *opo* mutants. We propose a model of retinal morphogenesis whereby *opo*-mediated formation of focal contacts is required to transmit the mechanical tensions that drive the macroscopic folding of the vertebrate optic cup.

KEY WORDS: Medaka fish, Optic cup, Organogenesis

INTRODUCTION

Visual acuity in chambered eyes relies on focusing light onto a hemispheric cup in which surface photoreceptors are arranged. In vertebrates, two consecutive morphogenetic events shape the primordium into a hemispheric structure (Schmitt and Dowling, 1994). The first step involves the lateral evagination of retinal progenitor cells (RPCs) to form optic vesicles. It has recently been reported that this step is driven by the individual migration of RPCs (Rembold et al., 2006), under the control of the transcription factor *Rx3* (Loosli et al., 2001). In a second series of morphogenetic events, the optic vesicles transform into the hemispheric bi-layered cup. Although extensive information is available regarding the initial specification and patterning of the eye anlage (Chow and Lang, 2001; Martinez-Morales et al., 2004b), the cellular and molecular mechanisms underlying optic cup folding remain largely unexplored. In particular, the dynamic movements that shape the optic cup have never been recorded in living embryos.

During organogenesis, spatial tissue rearrangements rely on a limited number of stereotypical cell behaviors that are exemplified by, at opposite extremes, individual cell migration and coordinated cell shape change (Locascio and Nieto, 2001; Pilot and Lecuit, 2005). At the molecular level, changes in the morphology of cells depend on the local organization of the cytoskeleton. In turn, cytoskeletal rearrangements depend on membrane polarization and compartmentalization, a consequence of cell-cell and cell-substrate interactions (Nelson, 2003).

In epithelial tissues, morphogenetic events along the apicobasal axis have a deep impact on macroscopic rearrangements. Apical constriction in polarized epithelia is the best studied of these phenomena, and involves the conversion of columnar cells into wedge-shaped cells. It is a common mechanism employed to bend cell sheets in several tissues in different organisms; for example, during gastrulation in *Drosophila* (Leptin, 2005) or neural tube closure in vertebrates (Wallingford, 2005). The molecular mechanism underlying apical constriction has been studied in detail in *Drosophila* and involves the recruitment of the acto-myosin cytoskeleton to the cellular cortex (Young et al., 1991). Both in *Drosophila* and in vertebrate epithelia, cell polarity depends on the local assembly of receptors and adaptor proteins. Three apical or sub-apical complexes, Crumbs/PATJ/Stardust, Par3/Par6/atypical protein kinase C (aPKC), and Scribble/Discs-Large/Lethal-Giant-Larvae, have been shown to be essential for epithelial polarization in all model organisms analyzed (Bilder, 2003; Nelson, 2003; Schock and Perrimon, 2002). The polarized distribution of some of these apical polarity determinants has also been reported in the developing neural retina (Malicki, 2004).

Cell polarization has also been linked to the interaction of cells with the extracellular matrix (ECM), which, in focal adhesions, is mainly mediated by transmembrane integrin receptors. Focal adhesions contain a number of integrin-associated scaffolding proteins (e.g. paxillin, vinculin, FAK) that act as an interface between the plasma membrane and the actin cytoskeleton (Burridge and Chrzanowska-Wodnicka, 1996; Turner, 2000). In contrast to the universal role of the above-mentioned apical determinants, the role of focal adhesions in cell polarity largely depends on the cellular context. Although it has been shown that integrins have no role in establishing the polarity of monostratified epithelial cells in *Drosophila* (Fernandez-Minan et al., 2007), they are required to

[1]Developmental unit and [3]Cell Biology unit, EMBL, Meyerhofstrasse 1, 69117 Heidelberg, Germany. [2]Centro Andaluz de Biología del Desarrollo (UPO/CSIC), 41013 Sevilla, Spain. [4]Max-Planck Institute for Molecular Genetics, Ihnestrasse 73, 14195 Berlin-Dahlem, Germany.

*Authors for correspondence (e-mails: jrmarmor@upo.es; Jochen.Wittbrodt@EMBL-Heidelberg.de)
†Present address: Centre for Genomic Regulation, UPF, 08003 Barcelona, Spain
‡Present address: HIZ, University of Heidelberg and ITG Forschungszentrum-Karlsruhe, c/o EMBL-Heidelberg, Germany

Accepted 22 April 2009

place general apicobasal determinants in the stratified epithelium of the mammalian epidermis (Lechler and Fuchs, 2005). We are still far from understanding how general cell polarity and cell adhesion are interconnected. Moreover, there is little information on how these complex cellular processes are coordinated to control the morphogenesis of an entire organ.

Here, we have identified the medaka (*Oryzias latipes*) mutation *ojoplano* (*opo*), which affects the morphogenesis of several epithelial tissues. We employ this morphogenetic mutant as a tool to understand the cellular mechanisms underlying eye formation. We provide a detailed comparative analysis of the morphogenetic movements underlying optic cup folding, as well as the polarity and cell shape dynamics of neuroblasts, in wild-type and in *opo* mutants. *opo* encodes an uncharacterized transmembrane protein that localizes to compartments of the secretory pathway and to neuropeithelial end-feet. We provide evidence that *opo* function is essential to localize focal adhesion components basally and that integrin function is required for optic cup morphogenesis. A single previous report in humans identified incomplete homologous transcripts of the gene within a locus linked to orofacial clefting hereditary disease (Davies et al., 2004). The craniofacial phenotype observed in medaka mutants further supports the link of *opo* to one of the most prevalent birth defects in humans.

MATERIALS AND METHODS

Fish stocks

Medaka (*Oryzias latipes*) wild-type strains Cab and Kaga were kept as described (Koster et al., 1997). The Kaga strain was used for chromosomal assignation and positional cloning. Embryos were staged according to Iwamatsu (Iwamatsu, 1994).

Selective plane illumination microscopy (SPIM) and confocal time lapse analyses

Stage 23 *rx2::eGFP* embryos were immobilized in balanced salt solution (BSS; containing 0.01% tricaine and 3 mM heptanol) and embedded in 1% low-melting agarose. Time-lapse analysis was performed using SPIM (Huisken et al., 2004) with a Zeiss 40×/0.8W lens and a 488-nm laserline. Samples were imaged for more than 30 hours with a time resolution of 10 minutes. Several central planes, spanning 9 μm, were integrated using ImageJ (NIH). For 3D reconstructions, the information from full stacks was integrated using Imaris (Bitplane). For standard confocal microscopy, stage 23 *rx2::mYFP* embryos were immobilized. Time-lapse analyses were performed on a Leica TCS-SP5 microscope with a HCPlanApo20×/0.7NA objective and a 514-nm laserline. At each time point, three optical sections spanning 3 μm were integrated using Imaris. Samples were imaged with a time resolution of 2 minutes.

Genetic mapping and positional cloning

opo was assigned to chromosome 20 by bulk segregation analysis (Martinez-Morales et al., 2004a). The genetic distance to the locus was narrowed by testing genetic markers (Naruse et al., 2000) on 1296 mutant chromosomes. We used the markers Ola2311a (8/1296; 0.6 cM) and Ola4805 (7/1296; 0.5 cM) as references flanking the mutation. From these anchoring points, chromosomal walking defined an 85-kb interval (0/1296) containing *opo*. All genetically mapped positions were confirmed at Ensembl (Kasahara et al., 2007).

BAC, cDNA and morpholino injections

Rescue experiments were performed using the BACs Hd228o24, Hd195c24 and Hd219g12 (Khorasani et al., 2004). Purified BACs were injected (10-30 ng/ul) into one-cell stage embryos. For tissue-specific cDNA rescue, *rx2::opo* plasmid was injected (20 ng/μl) into one-cell stage embryos using the meganuclease approach (Thermes et al., 2002). Splicing morpholinos were obtained from Gene Tools. The following morpholinos were injected:

MOm-opoEx18a, 5′-TGGGTCCAGCTGGTGCTGACctgtt-3′ (250-500 μM);

MOm-opoEx3d, 5′-tcatcaagcaggactcacccaTCAG-3′ (100-300 μM); and MOz-opoEx3d, 5′-ggactcacccaTCAGAAATTCAGCC-3′ (300 μM).

opo exon 18 skipping resulted in protein destabilization, as assessed by western blot (not shown).

opo gene structure and mutation

The complete gene structure of *opo* was deduced by 3′ and 5′ RACE (SMART-RACE, Clontech). Eight different primers were used for the 5′ and 3′ RACE (sequences are available upon request). 5′ RACE reactions detected a single 5′ end (also confirmed using GeneRacer, Invitrogen). The 3′ race detected several splicing isoforms, further confirmed by RT-PCR. EMBL accession numbers AM920650 and AM920651 correspond to the long and short isoforms, respectively. For RT-PCRs, total RNA was extracted (TRIzol, Invitrogen) and reverse transcription reactions were performed (Super Script III, Invitrogen). A 3′ fragment of the chicken *Opo* homolog was also isolated by RT-PCR (EMBL accession number AM920652). The 24 exons of *opo* and their flanking genomic regions were sequenced from heterozygous parents and their mutant progeny. Although several polymorphisms were detected, no mutation was identified. *opo* cDNAs derived from wild-type and mutant embryos were also compared. The anomalous *opo* splicing variant in exon 4 was never observed in wild-type embryos (20 independent cDNAs were analyzed), but was detected in four out of seven mutant full-length cDNAs analyzed. Examination of flanking introns 3 and 4, both in heterozygous parents and mutant progeny, revealed an insertion of two base pairs in intron 4 that correlates with the mutation. The insertion is located 715 bp 3′ of the affected splicing acceptor in the sequence:

Wild type, 5′-TTGATTTATTTATTTTTATTGCTTTTGCGCTAAA-AGGTT-3′;

Mutant, 5′-TTGATTTATTTATT***TA***TTTATTGCTTTTGCGCTAAA-AGGTT-3′.

This sequence contains a branch point sequence (underlined) and a polypyrimidine tract. Moreover, the 10-bp wild-type motif ATTTATTTTT disrupted by the insertion (in bold italics) is conserved in intron 4 of teleosts (Fugu, Tetraodon and Stickleback). These observations suggest that the disrupted region has a conserved regulatory role related to local assembly of the spliceosome complex.

Transmembrane topology prediction

Transmembrane predictions were performed at Sosui [http://bp.nuap.nagoya-u.ac.jp/sosui (Hirokawa et al., 1998)] and Phobius [http://phobius.sbc.su.se (Kall et al., 2004)].

Transgenics and constructs

Stable lines *rx2::eGFP* and *rx2::mYFP* were generated by ET-recombination (Muyrers et al., 1999). Both *eGFP* and *mYFP* (Clontech) were introduced in a cosmid containing the *rx2* gene, 4 amino acids downstream of the ATG start site.

Expression constructs were cloned into I-SceI vectors, and injected (10-20 ng/μl) into one-cell stage embryos (Thermes et al., 2002). To generate the *tyr::eGFP* construct, a 3-kb promoter fragment of medaka *tyrosinase* was fused to *eGFP*. The vectors *rx2::opo* and *rx2::opoGfp* were cloned, using Gateway technology (Invitrogen) by inserting *opo* and *opo:GFP* into the *rx2* destination vector. The *rx2* destination vector was generated by inserting a 2.4-kb fragment of the medaka *rx2* promoter upstream of a gateway destination cassette in the I-SceI transgenesis vector. *vsx3:Intβ1tail-eGFP* and *vsx3::torso^{D}/βcyt* were generated by cloning the fusions *Intβ1tail:eGFP* and *torso^{D}/βcyt* under the control of the retinal specific *vsx3* promoter (5-kb fragment upstream of the *vsx3* ATG). *Intβ1tail:eGFP* was generated by cloning *eGFP* at the C terminus of the 70 C-terminal amino acids of the *Drosophila* integrin beta PS. The dominant-negative *torso^{D}/βcyt* construct was reported previously (Martin-Bermudo and Brown, 1999). The medaka *vsx3::OLint-β1Δ21* construct is equivalent to a human dominant-negative variant, previously shown to interfere with cell adhesion to laminin (Retta et al., 1998). Fusion proteins (zebrafish) *ASIP/par3:eGFP* (von Trotha et al., 2006) and *pEGFPC1-(avian) paxillin WT1-559* (West et al., 2001) were subcloned into *pCS2+*. Capped sense RNAs were synthesized in vitro (mMessage Machine, Ambion). Purified RNA was then injected (50-100 ng/μl) into one-cell stage embryos.

Antibodies and molecular probes

Antibodies against Opo protein were generated by immunizing animals with purified recombinant GST-fusions. *opo* fragments encoding either the 112 N-terminal or the 183 C-terminal amino acids of the protein were cloned into *pGEX-KG* for expression. Purified GST:opo-N and GST:opo-C were employed to generate both mono and polyclonal antibodies. Polyclonal anti:opo-N was employed in immunostainings at a dilution of 1:500. The following commercial primary antibodies and molecular probes were used: anti-paxillin monoclonal antibody at 1:300 (BD Biosciences); polyclonal anti-phosphorylated histone H3a at 1:500 (Upstate Biotechnology); polyclonal anti-γ-tubulin at 1:500 (Sigma T5192); polyclonal anti-laminin at 1:500 (Sigma L9393); monoclonal anti-acetylated tubulin at 1:1000 (Sigma T6793); monoclonal anti-α-tubulin at 1:1000 (Sigma T9026); polyclonal anti-PKCζ (C-20) at 1:1000 (Santa Cruz Biotechnology); polyclonal anti-calnexin (Stressgen) at 1:1000; monoclonal anti-GM130 (BD Biosciences) at 1:250; monoclonal anti-integrin β/CD29 (Epitomics); phalloidin Alexa-488 (Invitrogen) at 1:10.

Western blot

Embryo heads were homogenized in 5% β-mercaptoethanol, 2% SDS, 1 mM PMSF (phenylmethylsulphonyl fluoride) and 50 mM Tris-HCl (pH 6.8). Supernatants were separated by SDS-PAGE (20 μg of protein per lane) and transferred to nitrocellulose membranes, blocked with 5% non-fat dry milk in PBT (PBS, 0.1% Tween) and probed with primary antibodies [anti:α-tubulin monoclonal (1:1000); anti:opo-N monoclonal supernatant (1:20) and anti:opo-C polyclonal (1 ug/ml)]. Blots were developed using peroxidase-conjugated anti-rabbit or anti-mouse antibodies (1:7000, Jackson). Antibody binding was visualized using the ECL system (Amersham).

Immunohistochemistry and histological staining

Embryos were fixed in 4% paraformaldehyde-PBS overnight at 4°C, equilibrated in 30% sucrose in PBS, embedded in OCT compound and sectioned at 18 μm using a cryostat (Leica). Tissue was blocked for 1 hour in PBS 0.1% Tween (PBT) and 10% FCS. Primary antibodies diluted in PBT-10% FCS were added overnight at 4°C. After washing in PBT, sections were incubated with Alexa-conjugated (Molecular Probes) secondary antibodies for 1 hour. Fluorescence sections were mounted with PBS/glycerol and analyzed with a confocal imaging system (TCS SP2, Leica). For cortical actin staining, sections were washed with PBS/Triton (0.1% Triton X-100) and incubated with phalloidin Alexa-488 (diluted 1:10 in 5% DMSO) in PBS/Triton overnight at 4°C. Methylene Blue-Azure II stainings were performed as described (Loosli et al., 2004).

Colocalization experiments in HeLa cells

Cells were transfected with *CMV::opoGfp* (FuGENE6, Roche) and allowed to express for 24 hours at 37°C. Cells were then fixed in ice-cold (–20°C) methanol for 4 minutes, washed with PBS, then incubated with appropriate dilutions of primary antibodies for 30 minutes and secondary antibodies labelled with Alexa-568 for 30 minutes. After PBS washing, cells were mounted in Moviol and images acquired on a Zeiss Axiovert200 microscope.

In situ hybridization

In situ hybridization was performed using digoxigenin riboprobes as described (Martinez-Morales et al., 2005). A 3′ *opo* probe common to all isoforms was used. For vibratome sections, embryos were embedded in gelatin/albumin and sectioned at a thickness of 30 μm (Leica).

Transplants

Cell transplantation was done as described (Rembold et al., 2006). Briefly, embryos were dechorionated with proteinase K (10 mg/ml in H_2O) and hatching enzyme, and maintained on dishes coated with 1% agarose/BSS. At blastula stage (stage 10/11), approximately 20-40 cells were transplanted from donors into the animal pole of host embryos (either wild-type or *opo* mutants). The development of both labelled donors (*rx2::eGFP*) and unlabelled hosts was followed for phenotypical assessment at stages 24 to 26.

Statistical analysis

Quantitative data are expressed as mean±s.e.m. Significant differences were evaluated by two-way ANOVA with Bonferroni post-hoc tests (GraphPad Prism) and are indicated when significant.

RESULTS

Morphogenesis but not tissue patterning is altered in *opo* embryos

In a large-scale ENU mutagenesis screen in medaka (Loosli et al., 2004), we identified *ojoplano* (*opo*), a mutant that affects the morphogenesis of several epithelial tissues. *opo* is a recessive lethal mutation with full penetrance and minimal phenotypical variability. Mutant embryos first become apparent at the onset of optic cup folding (stage 23), by virtue of their abnormal retinal morphology. Later during organogenesis, additional morphogenetic defects were observed in the brain, heart, fins, craniofacial region and eye. The ocular phenotype was particularly prominent, giving rise to the name: *ojoplano*, 'flat eye' in Spanish. As development proceeds, mutant optic vesicles fail to fold properly, resulting in a large ventral opening (Fig. 1A,B). Moreover, retinal ganglion cell axons exit the misshapen optic cup ventrally in defasciculated bundles (Fig. 1C,D). Despite the mutant eye morphology, RPC proliferation, neuronal differentiation and retinal lamination were normal at late organogenesis stages (Fig. 1E,F; see also Fig. S1A in the supplementary material). In addition, the lens, despite its abnormal morphology, was correctly specified (see Fig. S1A in the supplementary material). The abnormal shape of the optic cup is not a consequence of a failure in ventral retina specification. Known ventral markers were normally expressed in mutant retinae (see Fig. S1B in the supplementary material; data not shown), indicating that patterning is not altered in *opo* mutants.

As with the eye phenotype, none of the other morphogenetic defects observed in *opo* mutants were associated with patterning failures. Despite their correct initial specification, neural crest cells failed to migrate/delaminate (see Fig. S2A in the supplementary material). Consequently, neural crest derivatives are reduced or absent in *opo* mutants. Similarly, despite the correct specification of fin bud mesenchyma, the apical ectodermal ridge was misshaped. As a result, pectoral fins fail to grow properly (see Fig. S2C in the supplementary material). These deficiencies indicate a general role for the mutated gene in epithelial morphogenesis. Here, we focus on optic cup folding to gain insight into the function of *opo* in tissue morphogenesis.

A series of morphogenetic events shapes the vertebrate optic cup

To gain insight into the cellular mechanisms shaping the vertebrate eye, we followed optic cup morphogenesis in vivo in wild-type and mutant embryos. By using an eye-specific transgenic line, *rx2::eGFP*, that labels all RPCs, eye folding was followed by SPIM (Huisken et al., 2004). Both wild-type and *opo* retinae were imaged through the transition from optic vesicle to optic cup (30 hours, stages 22 to 27). At each time point, a complete stack of images spanning the whole retina was recorded from a lateral perspective. Three-dimensional renderings show that, although epithelial folding occurs in mutant retinae along the dorsoventral axis, it is not even initiated along the anteroposterior axis (Fig. 1G,H).

To visualize the process clearly, we generated projections of several slices at the level of the lens. In wild-type retinae, the initial folding of the epithelium occurs rapidly (see Movie 1 in the supplementary material). After 6 hours, as the tissue grows and anterior and posterior borders of the sheet bend ventrally, the eye primordium was already folded into a hemisphere. Despite this, the final ventral fusion of retinal borders, sealing the optic fissure, was not complete after 40 hours of recording (stage 27). In *opo* retinae, the epithelial sheet, although growing along the anteroposterior axis, does not bend ventrally even after 33 hours of development (see

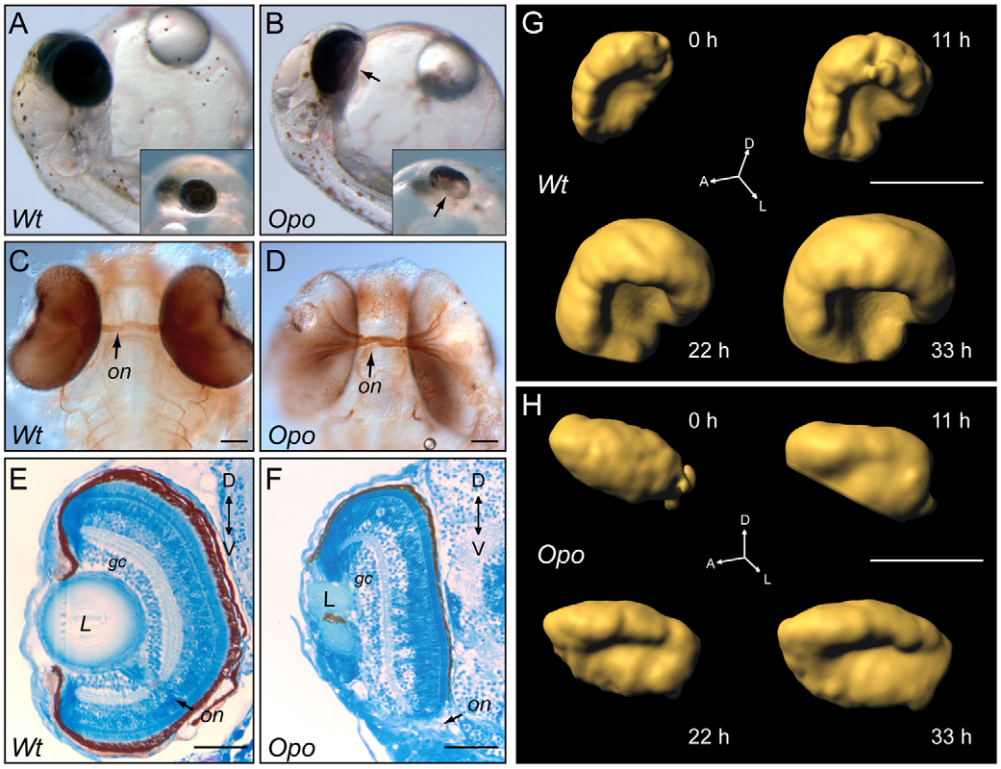

Fig. 1. The *opo* mutant affects optic cup morphogenesis. (**A**,**B**) Medaka wild-type (A) and *opo* mutant (B) embryos at stage 36. Arrows indicate ventral opening of the optic cup in *opo* mutants. Insets show a ventral view of the eye through the yolk. (**C**,**D**) Fasciculation of the optic nerve (on) shown by acetylated tubulin staining of wild-type (C) and opo mutant (D) embryos at stage 34. (**E**,**F**) Retinal differentiation and lamination in *opo* mutants, as shown by Methylene Blue-stained sections. (**G**,**H**) Three-dimensional renderings obtained from SPIM time-lapse analyses show both wild-type (G) and *opo* mutant (H) *rx2::Gfp* transgenic eyes at four different time points during optic cup folding. Scale bars: 100 μm. gc, ganglion cell layer; L, lens; on, optic nerve.

Movie 2 in the supplementary material). The clear temporal separation of cup folding and fissure closure thus indicates that these are distinct events with independent mechanisms.

ojoplano encodes an uncharacterized transmembrane protein

We mapped the *opo* locus to chromosome 20 by bulk segregation analysis (Martinez-Morales et al., 2004a) and identified the mutated gene by BAC walking (Fig. 2A). The locus sits in a 400-kb gene desert and includes a 70-kb transcription unit with homology to an uncharacterized human gene. Incomplete transcripts of this gene have been described in humans, and the locus has been proposed as being causative for orofacial clefting syndrome (Davies et al., 2004). The complete structure of the medaka gene, termed *ojoplano* (*opo*) after the mutation, was deduced by 3′ and 5′ RACE (Fig. 2A). The gene comprises 24 exons (3568 bp in total), and is transcribed into several splicing isoforms. *opo* transcripts do not encode any known protein domain. Orthologous genes can be identified in syntenic regions of all of the vertebrate genomes available (see Fig. S3A in the supplementary material). Two conserved regions were found: a 90-amino acid N-terminal domain, which corresponds to exons 3 to 5, and a 230-amino acid C-terminal domain, corresponding to exons 18 to 22. Transmembrane topology prediction algorithms identified four putative transmembrane helices in the conserved carboxy domain, orienting both termini of the protein towards the cytoplasm (see Fig. S3B in the supplementary material). Using either monoclonal antibodies against the N terminus (Fig. 3B, Fig. 4A) or polyclonal antibodies against the C terminus (not shown), we identified two isoforms by western blot: a 130-kDa band, corresponding to a 1091-amino acid protein encoded by an mRNA spanning all exons, and a 42-kDa band, corresponding to the skipping of the intermediate exons 5 to 16.

The injection of BAC Hd228o24, covering the *opo* locus, into the offspring of a carrier-cross resulted in a rescue efficiency of 36% (Fig. 2B). In addition, we observed an intermediate phenotype never present in uninjected carrier-crosses: a partial rescue of the facial phenotype and/or asymmetric rescue of the fins. To unambiguously confirm the identity of the causative gene, we placed *opo* cDNA under the control of the eye specific promoter *rx2* (*rx2::opo*). Injection of this construct efficiently rescued the mutant phenotype in a tissue specific manner: 52% of the *opo* mutant embryos identified by their fin phenotype developed wild-type eyes (Fig. 2C).

A splicing defect is the cause of the *opo* hypomorphic phenotype

We detected an anomalous splicing variant in *opo* mutants that was never observed in wild type. In mutants, four out of seven *opo* cDNAs analyzed used an alternative splice-acceptor in exon 4, skipping the first four nucleotides of the exon. This introduces a frameshift that results in a premature stop codon and leads to a truncated protein of 40 amino acids (Fig. 3A). In mutant embryos, we detected an insertion of two base pairs in intron 4 that is linked to the atypical splicing (see Materials and methods). As a consequence, Opo protein levels are reduced to 20% of wild-type levels for the 130-kDa full-length protein, and to 60% of wild-type levels for the 42-kDa isoform, as detected by western blot (Fig. 3B). These data indicate that the mutation is hypomorphic and that the observed phenotype is due to insufficient synthesis of wild-type protein.

To understand the phenotypical consequences of a progressive decrease of *opo* function, we performed morpholino injection experiments. Morpholinos interfering with the splicing of exon 18 were injected into *rx2::mYFP* embryos to examine the optic vesicle phenotype. Injected embryos were classified either as wild type-like, *opo*-like or strongly affected (Fig. 3C). *opo*-like morphants phenocopied mutants: eye folding did not occur, and craniofacial and

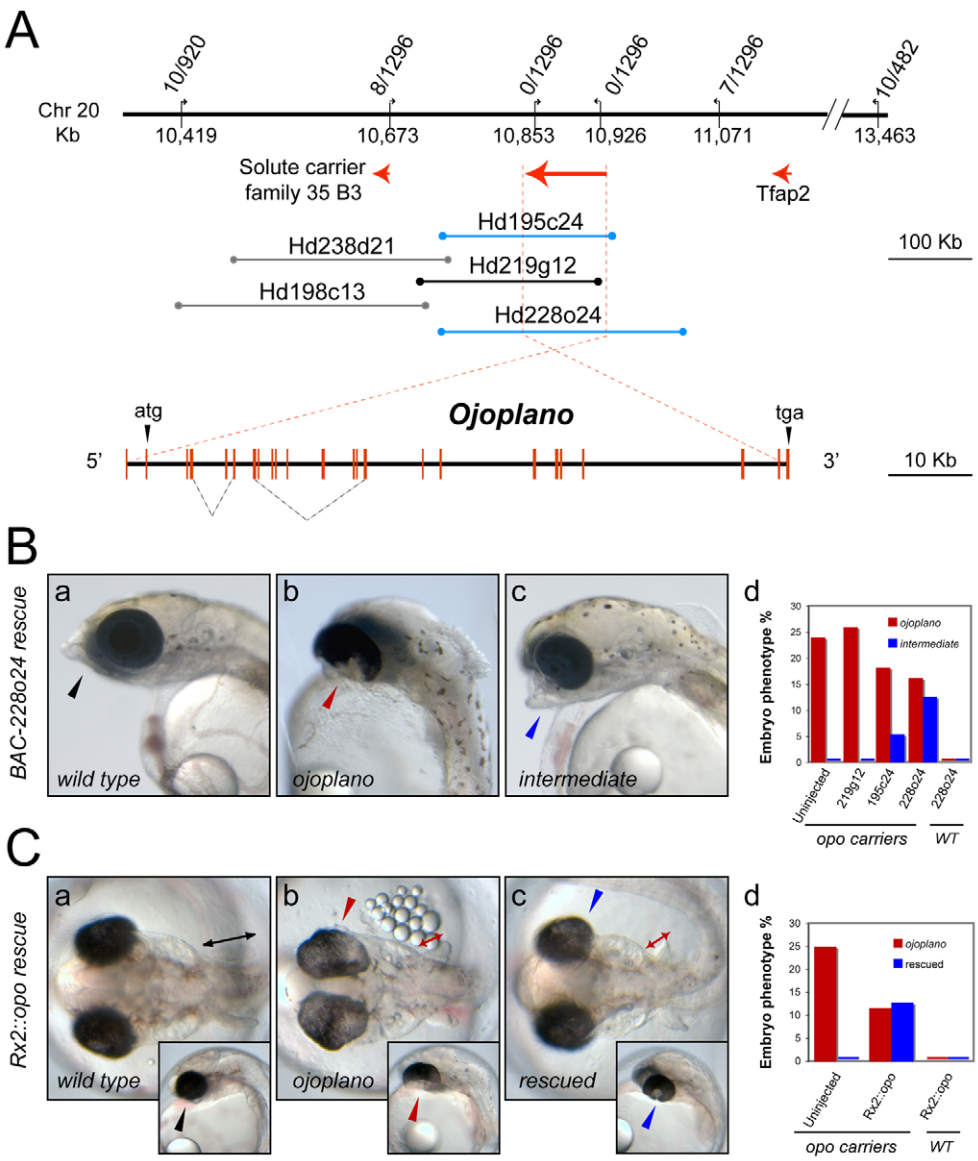

Fig. 2. *opo* cloning, gene structure and phenotypical rescue. (**A**, top) Genetic and physical map of the medaka *opo* locus on chromosome 20. Recombinants are indicated above and physical distance below the chromosome line. Transcription units are depicted as red arrows. BACs used for mapping are indicated. (Bottom) The genomic structure of *opo* is depicted; exons are represented as red bars; alternative splicing is shown by dotted lines. (**B**) Phenotypical rescue upon injection of BACs covering (Hd195c24 and Hd228o24) or not covering (Hd219g12) the *opo* locus. Wild-type (a), *opo* mutant (b) and intermediate (c) phenotypes were observed at stage 38. The percentage of embryos showing each phenotype is represented (d). Arrowheads highlight facial and ocular phenotypes. (**C**) Tissue-specific phenotypical rescue upon *rx2::opo* injection. Wild-type (a), *opo* (b) and rescued (c) phenotypes were observed at stage 32. The proportion of embryos showing each phenotype is shown (d). Double-headed arrows indicate the size of the fins; arrowheads indicate ocular phenotypes. See Tables S1 and S2 in the supplementary material.

fin malformations developed. In strongly affected morphants, the optic vesicles did not evaginate fully and remained fused at the midline (Fig. 3C). Molecular analysis of the phenotypical groups showed a direct correlation between the severity of the phenotype and the skipping of exon 18 (Fig. 3D). Taken together, our results demonstrate that the progressive loss of *opo* function induces an increasingly severe morphogenetic phenotype, which indicates a requirement of Opo at different levels for different morphogenetic processes.

Similar phenotypes were obtained upon injection of a second morpholino blocking the splicing between exons 3 and 4 (see Table S3 in the supplementary material). Moreover, in parallel interference experiments in zebrafish, the injection of morpholinos against the exon 3/4 junction caused a phenotype similar to that of medaka *opo*: a failure of optic vesicle folding (see Fig. S4 in the supplementary material).

opo localizes mainly to the ER and to neuroepithelial end-feet

To study Opo regulation during embryogenesis, we investigated its developmental profile by western blot. At stage 10, prior to the onset of zygotic transcription, maternal Opo protein was detected in embryo extracts. Protein levels decreased at late gastrula stages and increased during organogenesis, peaking at stage 26 (Fig. 4A). The spatial expression pattern of *opo* was investigated by in situ hybridization. At stage 26, both in wild type and in mutant embryos, *opo* was expressed in all tissues affected by the mutation, including eye, brain and neural crest precursors (Fig. 4; see also Fig. S5 in the supplementary material). Interestingly, transcripts are localized at the basal side of the pseudo-stratified epithelium of the developing retina both in wild-type and in *opo* mutant embryos (Fig. 4B,C). Furthermore, this localization is not exclusive to the medaka retina, as we could detect a similar distribution of the chicken homologous transcript at the basal surface of the optic vesicle epithelium (see Fig. S5C in the supplementary material). To explore the subcellular localization of the Opo protein, we expressed a GFP-tagged *opo* gene under the control of the eye-specific promoters *rx2* and *vsx3*. In transient *rx2::opoGfp* clones, Opo-GFP decorated the nuclei and also localized to the membranes of the basal cytoplasmic feet (Fig. 4D). In vivo examination of protein distribution in the stable *vsx3::opoGfp* line also revealed a preferential localization of Opo-GFP to the basal side of the epithelium (Fig. 4E), particularly to the tips of the neuroepithelial feet (Fig. 4F). Opo enrichment at the basal surface was further confirmed by

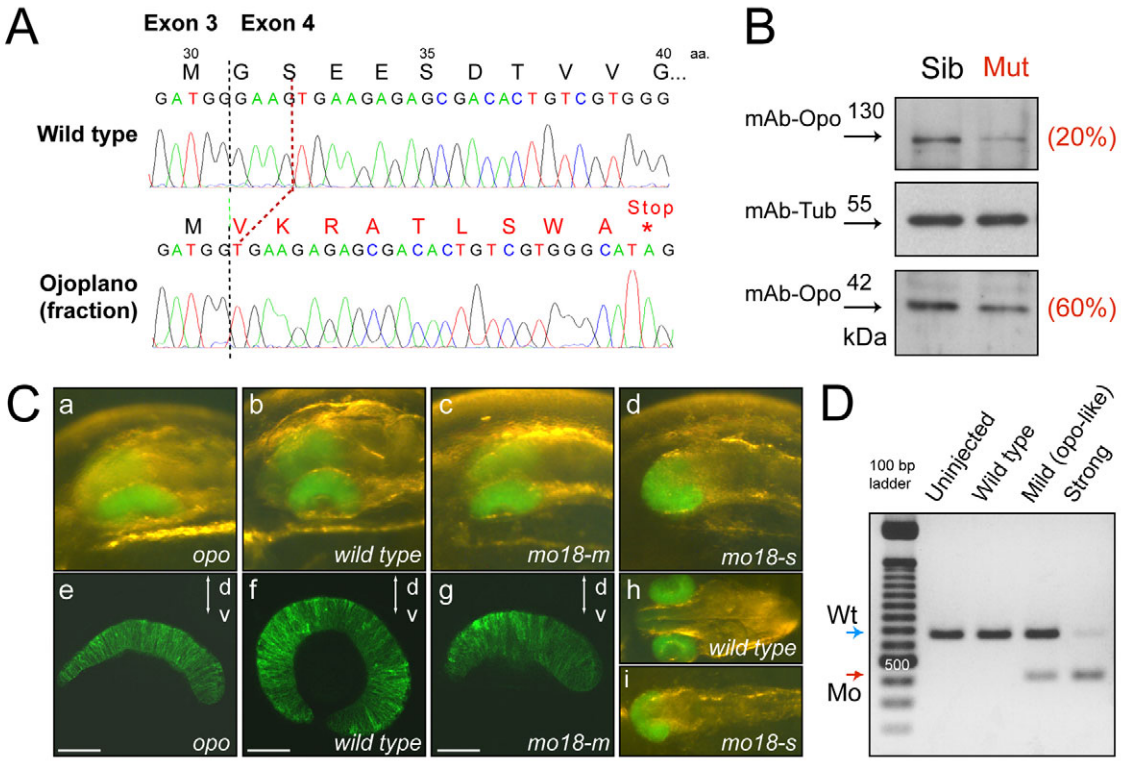

Fig. 3. *ojoplano* splicing defect and morpholino phenocopy. (**A**) The exon 3/4 junction is depicted for wild-type and mutant transcripts. Encoded amino acids and premature stop in *opo* mutants are also indicated. (**B**) Western blot of Opo 130 and 42 kDa isoforms in head extracts from stage 26 mutants (Mut) and siblings (Sib). The percentage decrease in protein levels in the mutant is shown. α-Tubulin was included as loading control. (**C**) *rx2::mYFP* embryos showing retinal morphology for *opo* (a,e) and wild type (b,f,h), and morpholino-injected embryos with mild (i.e. *opo*-like; c,g) or strong (d,i) phenotype (see also Table S3 in the supplementary material). Shown are stage 23 embryos in lateral (a-d) and dorsal (h,i) view, and eye morphology at stage 26 assessed by confocal microscopy (e-g). Scale bars: 50 μm. (**D**) RT-PCR amplification correlates phenotype and skipping of exon 18 (red arrow).

immunostaining using polyclonal antibodies against the N terminus of the protein (see Fig. S5 in the supplementary material). The perinuclear distribution of Opo suggests that the protein localizes to the ER. Subcellular colocalization experiments in HeLa cells transfected with *CMV::opoGfp* showed a perinuclear and reticular distribution of the Opo-GFP fusion protein, which colocalized with the ER marker calnexin and showed some correlation with the golgi marker GM130 (Fig. 4F-K). These experiments indicate that Opo localizes to intracellular compartments of the secretory pathway, mainly to the ER.

Defective basal recruitment of focal adhesions components in *opo* mutants

Given the central importance of epithelial polarization to tissue morphogenesis, the question arises as to whether Opo might be involved in the control of polarity. In contrast to the more common apical constriction, optic cup morphogenesis entails the bending of an epithelial sheet around its basal side. Given that the neural retina is polarized in the apicobasal plane (Malicki, 2004), and that optic cup folding may be linked to polarity, we examined the localization of apical and basal determinants in wild-type and *opo* mutant retinae. At stage 23, Par3-GFP (von Trotha et al., 2006) was localized to the apical side of the retina (Fig. 5A), showing that RPCs are polarized before optic cup folding. A similar distribution was found in *opo* mutants (Fig. 5E). Normal segregation of apical determinants in *opo* mutants was further confirmed in sections of wild-type and mutant retinae stained for γ-tubulin, which labels apical centrosomes (Fig. 5B,C,F,G), and aPKC (not shown). By contrast, we observed striking differences between the basal cell surfaces of wild-type and *opo* mutant retinae. During optic cup folding, the feet of RPCs attach to the basal lamina of the retina and form an array of narrow parallel cytoplasmic extensions that nuclei do not enter (zone of nuclear exclusion, ZNE). Using an *rx2::mYFP* (membrane YFP) transgenic line, we examined this basal organization of the tissue in wild-type and *opo*. In contrast to the membrane array observed in wild type, the feet of *opo* mutant neuroblasts are wider and appear disorganized, and nuclei are found closer to the basal surface (Fig. 5E,J; see Fig. S6 in the supplementary material). Consistently, although cortical actin cytoskeleton recruitment, as visualized by phalloidin staining, was normal at the apical junctions in *opo* mutants, reduced actin deposition was observed at the ZNE (Fig. 5K,P). At the basal surface, cytoskeletal organization and epithelial polarization depend on integrin-mediated focal contacts (Bokel and Brown, 2002; Schock and Perrimon, 2002). Therefore, we examined the distribution of paxillin, a scaffolding protein that links integrin receptors to the cytoskeleton (Turner, 2000). In contrast to its basal localization in wild-type retinae, paxillin accumulated poorly at the basal side in the mutants, as shown by immunostaining (Fig. 5L,Q) or after *paxillin:gfp* mRNA injection (Fig. 5M,R). Similarly, integrin β1, an essential component of the main receptor for laminins and collagens (Hynes, 1992), was also reduced basally, as revealed both by immunostaining (Fig. 5N,S) and by the eye-specific transgenic line *vsx3::integrinβ1-eGFP*

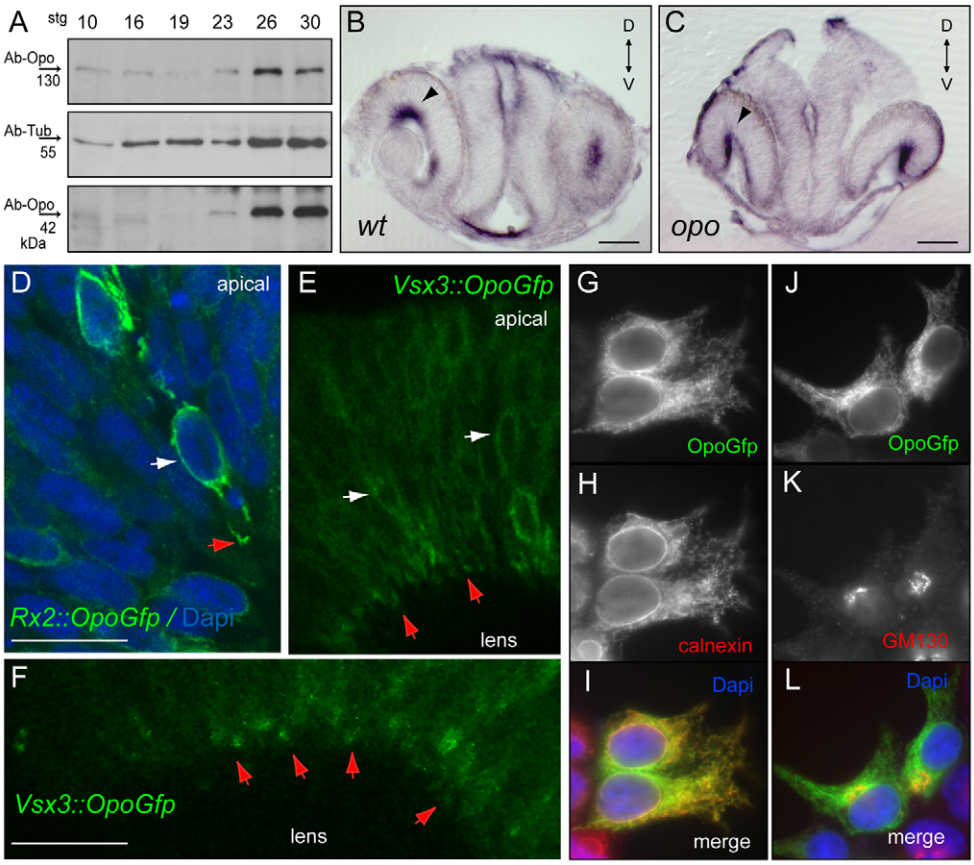

Fig. 4. Opo expression in the retina and subcellular localization of the protein. (**A**) Western blots show the regulation of Opo isoforms during development. Protein levels peak at organogenesis (stage 26). (**B**,**C**) *opo* expression in the stage 26 medaka retina by in situ hybridization. Sections reveal that transcripts are localized to the basal surface of the retina (arrowheads B,C). (**D**) Transient expression of *rx2::opoGfp* in the retina shows protein localization in the perinuclear compartment (white arrows) and basal feet (red arrows). (**E**,**F**) Stable *vsx3::opoGfp* line shows protein accumulation at the tip of the basal feet in vivo. (**G-L**) Opo protein localizes to the endoplasmic reticulum (ER) in HeLa cells. Cells transfected with the construct *CMV::opoGfp* (G,J) show a perinuclear and reticular distribution of the Opo-Gfp fusion, colocalising with the ER marker calnexin (H,I) and partially overlapping with the golgi marker GM130 (K,L). Scale bars: 50 μm in B,C; 20 μm in D,F.

(Fig. 5O,T). This deficient cortical recruitment of focal adhesion components is not a consequence of impaired basal lamina deposition, as laminin distribution was normal in mutant retinae (see Fig. S7A in the supplementary material). Furthermore, basal lamina integrity in *opo* mutant retinae was also confirmed by electron microscopy (see Fig. S7B in the supplementary material).

Optic cup folding depends on integrin-adhesive function

To assess whether focal adhesion formation has a role in optic cup morphogenesis, we interfered with integrin function by specifically expressing a dominant-negative construct in the eye anlage. We made use of the dominant-negative chimera *torso^{D}/βcyt*, which previously has been shown to interfere with integrin-adhesive function (Martin-Bermudo and Brown, 1999). Injection of this construct under the control of the eye-specific promoter *vsx3* (*vsx3::torso^{D}/βcyt*) in the reporter line *rx2::mYFP* impaired optic cup folding in 27% of the treated embryos (n=102). The optic cup morphogenetic defects observed in these embryos largely resembled those of *opo* mutants (Fig. 6A,B) and persisted to late stages (Fig. 6C,D). Similar defects were observed in 7% of the embryos injected (n=71) with a second dominant-negative construct, *vsx3::OLint-β1Δ21*, which lacks the last 21 cytoplasmic residues of medaka *integrin β1* (not shown). These experiments indicate that integrin-adhesive function is required for optic cup folding.

Nuclear morphology and basal surface dynamics suggest reduced tension in *opo* mutant cells

It is known that nuclei adapt their shape in response to the mechanical tension transmitted through the extracellular matrix (Maniotis et al., 1997). The defective basal organization of the *opo* mutant retina suggested that RPCs might not adhere well to the basal lamina, which would result in a reduction in the transmitted tension. In agreement with this idea, *opo* mutant nuclei appear round, in contrast to the elongated morphology observed in wild-type RPCs (Fig. 7A,B). We quantified changes in nuclear morphology during retinal morphogenesis by determining the ratio between the longer and shorter nuclear axes at several developmental stages (Fig. 7A-C). As the retina folds, nuclei progressively adopt an elongated shape in wild type but not in *opo* mutant retinae. This suggests that nuclear morphology serves as read-out of the tension exerted on RPCs. Alternatively, Opo protein could have a structural role in determining nuclear shape. To distinguish between these possibilities, the inability of individual cells to transduce tension or the inability of *opo* mutant nuclei to modify their shape, we performed transplantation experiments. In mosaic retinae (upon transplantation of either wild-type or *opo rx2::eGFP* cells) nuclear morphology was analyzed at stages 24 to 26. In control homotypic transplantations, nuclei of transplanted cells showed no changes in their morphology. By contrast, we observed an altered, elongated nuclear morphology in *opo* mutant clones in a wild-type context (Fig. 7E; ratio=2.34±0.11). Moreover, when wild-type cells were transplanted into an *opo* mutant host, they retained their elongated nuclear shape and rescued nuclear morphology in adjacent mutant cells (Fig. 7F; ratio=2.27±0.14). We can therefore rule out a cell-intrinsic function for Opo in regulating nuclear shape. Instead, these experiments suggest that, in the appropriate context, mutant cells can transduce tension provided laterally by neighboring wild-type cells. The round nuclear morphology would therefore represent an intrinsic failure of *opo* mutant cells to apply tension. To explore this further, we followed cell dynamics in vivo using *rx2::mYFP* transgenics. Cell shape changes were followed by time-lapse

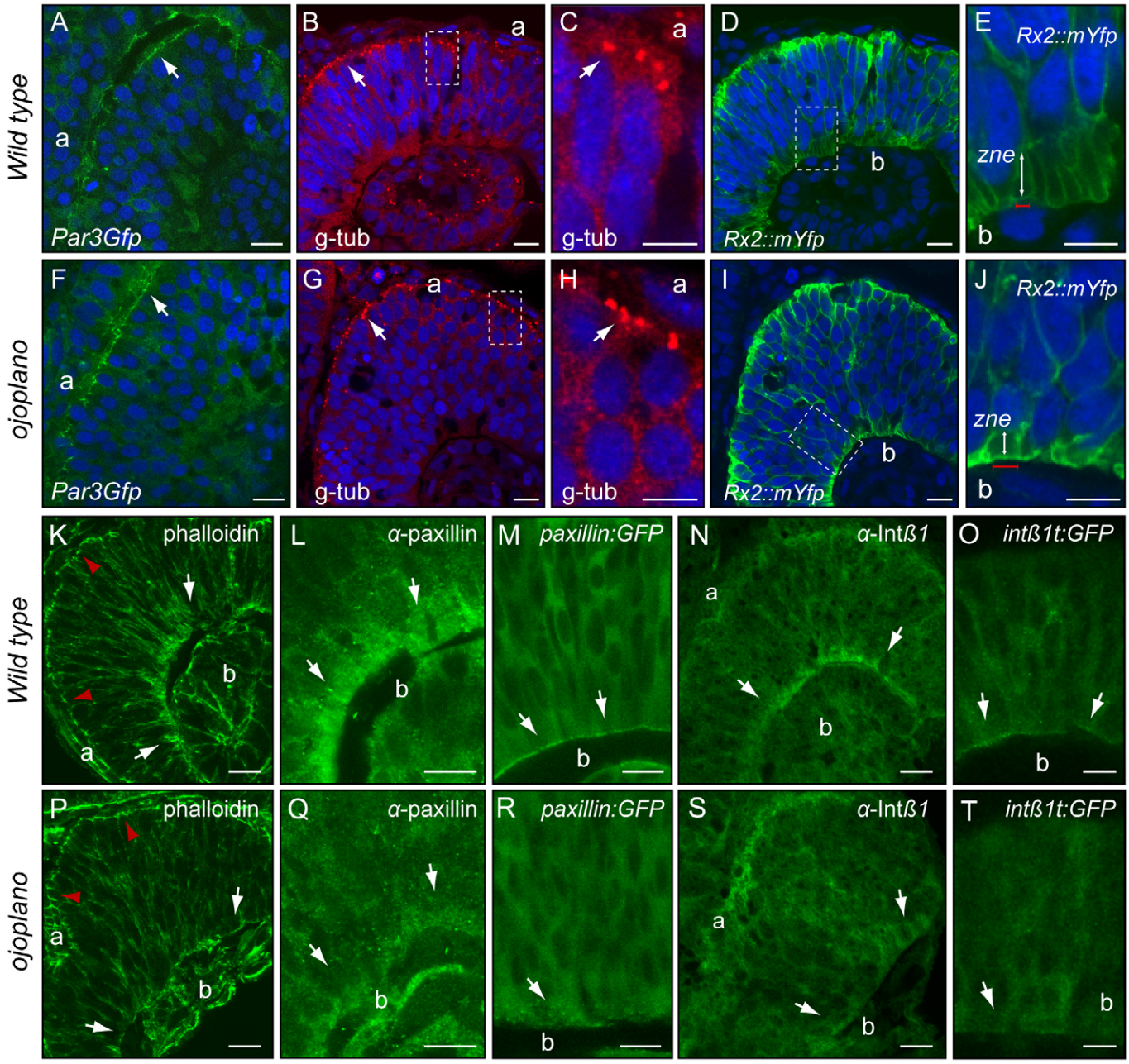

Fig. 5. Basal focal adhesion recruitment is deficient in *opo* mutants. (**A-J**) Apical (a) determinants are normally distributed in *opo* retinae. Par3Gfp (A,E) and γ-tubulin (B,C,F,G) were examined in retinal sections from stage 23 and stage 25 embryos, respectively. The abnormal morphology of neuroblast feet in *opo* mutants is highlighted by *rx2::mYfp* in stage 25 retinal sections (D,E,I,J). Double-headed arrows indicate zone of nuclear exclusion (zne). (**K-T**) Phalloidin staining reveals reduced recruitment of cortical actin at the basal (b; white arrows) but not the apical (red arrowheads) side in *opo* mutants (K,P). Focal adhesion components are greatly reduced at the zne in *opo* mutants. Endogenous paxillin (L,Q) and integrin β1 (N,S) were examined in stage 25 retinal sections. PaxillinGfp (M,R) and integrinβ1tailGfp (O,T) were examined in vivo in optical sections from stage 25 retinae. Scale bars: 10 μm in C,E,H,J; 20 μm in all other panels.

confocal microscopy over 3 hours at stage 23. Cells in wild-type retinae showed very active behavior at their basal side. Both filopodia and basal surface contractions were observed (see Movie 3 and Fig. S8 in the supplementary material). These dynamic contractions were not observed in the mutants (see Movie 4 and Fig. S8 in the supplementary material), suggesting that tension cannot be exerted properly at the basal surface when *opo* function is impaired (Fig. 7D).

DISCUSSION

A consecutive series of morphogenetic events shape the vertebrate optic cup

Because of its size and accessibility, the eye represents a paradigm for vertebrate organogenesis (Spemann, 1901). Here, we report the identification and characterization of the mutation *opo*, which affects epithelial morphogenesis and eye organogenesis in particular. Using time-lapse microscopy, we have characterized the series of events

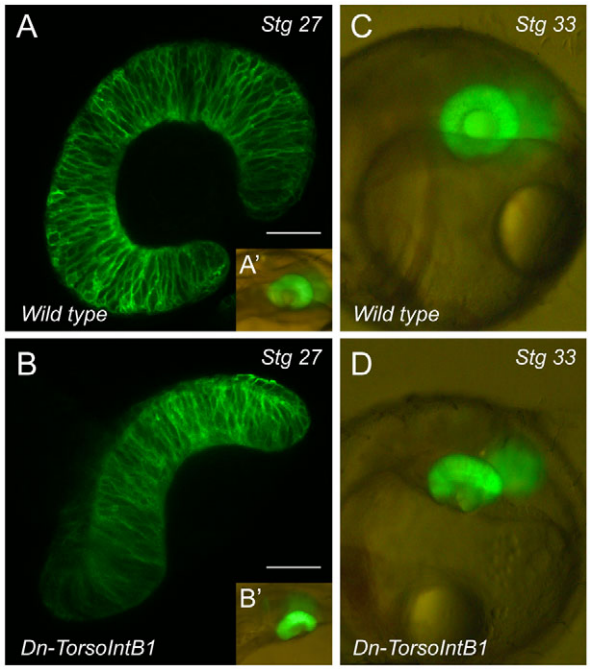

Fig. 6. Optic cup folding depends on integrin-adhesive function. Integrin function during optic cup morphogenesis was investigated by injecting the dominant-negative construct *vsx3::torso^{D}/βcyt* into the reporter line *rx2::mYFP*. Optical sections show optic cup morphology in wild-type (A) and *vsx3::torso^{D}/βcyt*-injected (B) embryos at stage 26. A′ and B′ show in toto embryos immediately before fixation. *torso^{D}/βcyt*-induced morphogenetic defects (D) are permanent, as assessed in stage 33 embryos (C), compare with wild type (D). Scale bars: 30 μm.

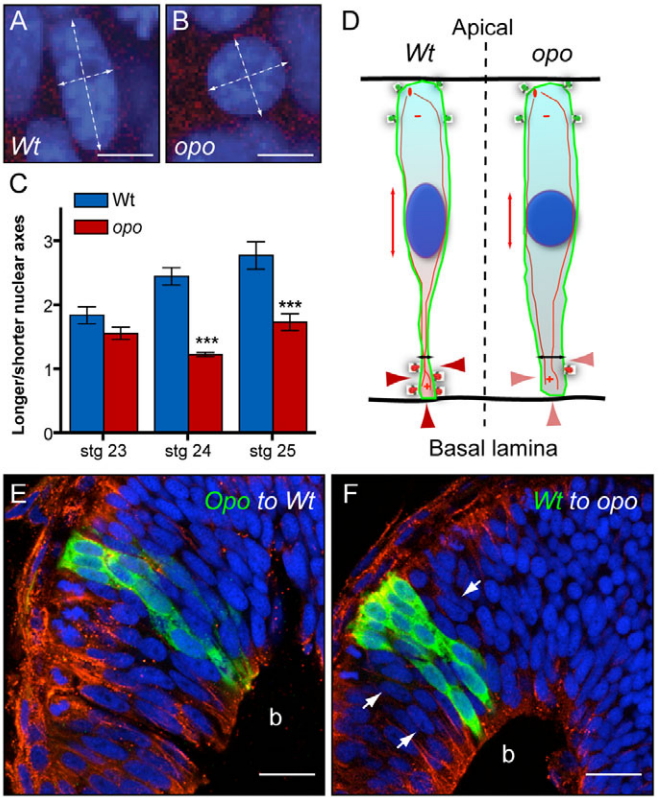

Fig. 7. Nuclear morphology and basal surface dynamics suggest reduced tension in *opo* mutant cells. (**A**,**B**) DAPI staining reveals different nuclear morphology in wild-type (A) and *opo* (B) RPCs. Dashed lines mark the longer and shorter nuclear axes. (**C**) The axes ratio changes significantly (n=12) as development proceeds in wild-type, but not mutant nuclei. (**D**) Model integrating microtubule orientation (±), polarity determinants (green, apical; red, basal) and nuclear morphology, proposing reduced basolateral tension (arrowheads) in *opo* mutants. (**E**,**F**) Mosaic retinae generated by transplanting Rx2::eGFP cells into unlabelled hosts. *opo* mutant cells show elongated nuclei in a wild-type context (E). Wild-type cells retain elongated morphology in an *opo* mutant context and rescue the nuclear morphology of *opo* mutant neighboring cells (arrows). Sections were counterstained with DAPI (blue) and anti α-tubulin (red). Scale bars: 10 μm in A,B; 20 μm in E,F.

involved in retina folding, and have determined when and how this morphogenetic process is impaired in *opo* mutants. We propose a three-step model for optic cup formation: anteroposterior folding, dorsoventral folding and optic fissure formation. The first morphogenetic event, which fails in *opo* mutants, folds the optic vesicle epithelium along its anteroposterior axis, bending the tissue ventrally so that the anterior and posterior borders converge. In a second, temporally overlapping event, the retinal tissue folds along the dorsoventral axis. This process is not affected in *opo* mutants, demonstrating that the two morphogenetic movements, although cooperative, have an independent genetic control. Once the hemispheric cup has formed, the third morphogenetic event involves the fusion of the optic cup borders and the ingression of cells from the ventral optic stalk region into the choroid fissure (Holt, 1980). Our analyses demonstrate that the folding of the optic cup and the formation of the optic fissure are consecutive events clearly separated in time. Several additional lines of evidence show that the early events shaping the cup and those forming the fissure later are genetically uncoupled. Although interference with the gene network that specifies the ventral retina often results in a failure to close the optic fissure (i.e. coloboma), these manipulations do not interfere with the formation of a hemispheric cup (Peters, 2002; Torres et al., 1996). Similarly, although optic disc formation is impaired in Bmp7-null mice because of a failure in the ventral ingression of Pax2^{+} cells, optic cup development occurs normally (Morcillo et al., 2006). Reciprocally, here, we show that the identity of the ventral retina is unaffected in *opo* mutant embryos despite the optic cup malformation.

An *opo*-mediated basal constriction is the driving force during optic cup morphogenesis

Here, we describe the isolation of a mutation in the *opo* gene. A mutant splicing isoform causes the premature truncation of the protein and subsequently reduces protein levels in *opo* embryos. Further reduction of protein levels by morpholino treatment causes a progressively stronger and earlier phenotype that resembles the lack of vesicle evagination observed in *Rx3* mutants (Loosli et al., 2001).

During optic cup formation, both *opo* transcripts and protein are basally localized, suggesting a role in cell polarity. We show that, despite the morphogenetic defects, apical marker localization, as well as cell proliferation and neuronal lamination (which both depend on apical identity), occur normally in *opo* mutants. This is in contrast to zebrafish mutants in which the localization of apical determinants is disrupted (Horne-Badovinac et al., 2001; Jensen and Westerfield, 2004; Malicki, 2004). Although cell cycle and lamination defects are reported in the retina of these mutants, the

organ shape appears unaffected. Interestingly, some zebrafish apical-polarity mutants show morphogenetic defects in the neural tube (Lowery and Sive, 2004). This is in agreement with the proposal that apical constriction is the morphogenetic mechanism involved in vertebrate neurulation (Wallingford, 2005).

In contrast to apical constriction, the basal bending of an epithelial sheet is a less studied phenomenon. Recently, basal constriction has been proposed as the driving force for the morphogenesis of the midbrain-hindbrain boundary (Gutzman et al., 2008). Here, we propose an *opo*-mediated basal constriction as the mechanism responsible for optic cup morphogenesis. We describe that, at the basal side of *opo* mutant retinae, neuroblast morphology is abnormal and cortical actin levels are reduced. Pioneering work has described optic cup folding as an active process that is dependent on ATP and Ca^{2+}, and potentially on a microfilament band (Brady and Hilfer, 1982). Our results show Opo protein accumulation at the ZNE, where cellular feet attach to the basal lamina forming a tight array of cytoplasmic extensions. Moreover, we show that the focal adhesion proteins integrin β1 and paxillin are not properly recruited to the ZNE in the mutants, suggesting that Opo functions to localize these crucial factors to the basal surface of RPCs. Specific interference with integrin-adhesive function indicates that focal contacts are required for optic cup folding, potentially by transmitting basolaterally the tensions that drive the epithelial bending. By analogy to what happens apically during neurulation, we propose that an active basal constriction, dependent on focal contacts, shapes the retinal epithelium into a hemispheric optic cup.

opo is a vertebrate innovation and a causative gene in human hereditary diseases

opo is present as a single copy in all of the vertebrate genomes that are available for searching. Blast and tblastn analyses against vertebrate genomes revealed two conserved regions: a 90-amino acids N-terminal motif and a 230-amino acid C-terminal motif that contains the predicted transmembrane passes. Whereas the C-terminal motif has homology with transcripts found in other metazoans (not protostomes), the N-terminal motif of the protein can be considered a vertebrate innovation. This fact and the fact that *opo* is expressed embryonically indicate that it is not a housekeeping gene but rather that it plays a regulatory role during development.

In humans, the *opo* ortholog sits in a large gene desert at the distal region of chromosome 6p. Deletions of this region cause a complex syndrome that includes mental retardation, abnormal brain sutures, heart defects, eye abnormalities and craniofacial malformations (Palmer et al., 1991). The extent to which the distal 6p deletion syndrome relates to the broader role of *opo* in epithelial morphogenesis requires further investigation. However there is already an established link between the *opo* ortholog in humans and the orofacial clefting syndrome (Davies et al., 2004). As medaka mutants also show strong craniofacial defects, they provide a model for understanding the underlying causality behind this common birth defect.

We thank Lazaro Centanin and Felix Loosli for their critical input; K. Naruse and H. Takeda for RFLP-markers; E. Marti, M. A. Rabadan and C. Funaya for the help with EM analyses; M. Souren for isolation the of *vsx3* promoter; V. Benes, T. Zimmermann and S. Terjung at the EMBL GeneCore facilities for methodological advice; A. M. Reugels and C. E. Turner for *par3:eGFP* and *GFP-Paxillin* constructs; and A. Nowicka, D. Hofmann, C. Müller and B. Wittbrodt for technical assistance. EMBO, Marie-Curie and Ramon y Cajal programs supported J.R.M.-M. This work was supported by grants from the Deutsche Forschungsgemeinschaft, Collaborative Research Centre 488, the EU and HFSPO to J.W.; and *MEC:BFU2008-04362/BMC* to J.R.M.-M. To the memory of Dr José-Santiago Martínez-Vinjoy.

Author contributions

The largest part of the work was done by J.R.M.-M. in J.W.'s and J.R.M.-M.'s laboratories. K.G. performed, with J.R.M.-M.'s help, the SPIM analyses. M.R.'s expertise and work was fundamental to the transplantation experiments. J.C.S. collaborated with J.R.M.-M. in elucidating the subcellular localization of Opo in R.P.'s laboratory. R.Q. generated the lines *rx2::eGFP* and *rx2::mYFP* by ET-recombination. M.D.M.-B. helped in the generation of the *vsx3:intβ1-eGFP* line and contributed to the discussions on integrin fuction. H.H.'s expertise facilitated the BAC-based chromosomal walking approach. The manuscript was written by J.R.M.-M. with the assistance of J.W. and K.E.B.

Supplementary material

Supplementary material for this article is available at
http://dev.biologists.org/cgi/content/full/136/13/2165/DC1

References

Bilder, D. (2003). PDZ domain polarity complexes. *Curr. Biol.* **13**, R661-R662.
Bokel, C. and Brown, N. H. (2002). Integrins in development: moving on, responding to, and sticking to the extracellular matrix. *Dev. Cell* **3**, 311-321.
Brady, R. C. and Hilfer, S. R. (1982). Optic cup formation: a calcium-regulated process. *Proc. Natl. Acad. Sci. USA* **79**, 5587-5591.
Burridge, K. and Chrzanowska-Wodnicka, M. (1996). Focal adhesions, contractility, and signaling. *Annu. Rev. Cell Dev. Biol.* **12**, 463-518.
Chow, R. L. and Lang, R. A. (2001). Early eye development in vertebrates. *Annu. Rev. Cell Dev. Biol.* **17**, 255-296.
Davies, S. J., Wise, C., Venkatesh, B., Mirza, G., Jefferson, A., Volpi, E. V. and Ragoussis, J. (2004). Mapping of three translocation breakpoints associated with orofacial clefting within 6p24 and identification of new transcripts within the region. *Cytogenet. Genome Res.* **105**, 47-53.
Fernandez-Minan, A., Martin-Bermudo, M. D. and Gonzalez-Reyes, A. (2007). Integrin signaling regulates spindle orientation in Drosophila to preserve the follicular-epithelium monolayer. *Curr. Biol.* **17**, 683-688.
Gutzman, J. H., Graeden, E. G., Lowery, L. A., Holley, H. S. and Sive, H. (2008). Formation of the zebrafish midbrain-hindbrain boundary constriction requires laminin-dependent basal constriction. *Mech. Dev.* **125**, 974-983.
Hirokawa, T., Boon-Chieng, S. and Mitaku, S. (1998). SOSUI: classification and secondary structure prediction system for membrane proteins. *Bioinformatics* **14**, 378-379.
Holt, C. (1980). Cell movements in Xenopus eye development. *Nature* **287**, 850-852.
Horne-Badovinac, S., Lin, D., Waldron, S., Schwarz, M., Mbamalu, G., Pawson, T., Jan, Y., Stainier, D. Y. and Abdelilah-Seyfried, S. (2001). Positional cloning of heart and soul reveals multiple roles for PKC lambda in zebrafish organogenesis. *Curr. Biol.* **11**, 1492-1502.
Huisken, J., Swoger, J., Del Bene, F., Wittbrodt, J. and Stelzer, E. H. (2004). Optical sectioning deep inside live embryos by selective plane illumination microscopy. *Science* **305**, 1007-1009.
Hynes, R. O. (1992). Integrins: versatility, modulation, and signaling in cell adhesion. *Cell* **69**, 11-25.
Iwamatsu, T. (1994). Stages of normal development in the medaka Oryzias latipes. *Zool. Sci.* **11**, 825-839.
Jensen, A. M. and Westerfield, M. (2004). Zebrafish mosaic eyes is a novel FERM protein required for retinal lamination and retinal pigmented epithelial tight junction formation. *Curr. Biol.* **14**, 711-717.
Kall, L., Krogh, A. and Sonnhammer, E. L. (2004). A combined transmembrane topology and signal peptide prediction method. *J. Mol. Biol.* **338**, 1027-1036.
Kasahara, M., Naruse, K., Sasaki, S., Nakatani, Y., Qu, W., Ahsan, B., Yamada, T., Nagayasu, Y., Doi, K., Kasai, Y. et al. (2007). The medaka draft genome and insights into vertebrate genome evolution. *Nature* **447**, 714-719.
Khorasani, M. Z., Hennig, S., Imre, G., Asakawa, S., Palczewski, S., Berger, A., Hori, H., Naruse, K., Mitani, H., Shima, A. et al. (2004). A first generation physical map of the medaka genome in BACs essential for positional cloning and clone-by-clone based genomic sequencing. *Mech. Dev.* **121**, 903-913.
Koster, R., Stick, R., Loosli, F. and Wittbrodt, J. (1997). Medaka spalt acts as a target gene of hedgehog signaling. *Development* **124**, 3147-3156.
Lechler, T. and Fuchs, E. (2005). Asymmetric cell divisions promote stratification and differentiation of mammalian skin. *Nature* **437**, 275-280.
Leptin, M. (2005). Gastrulation movements: the logic and the nuts and bolts. *Dev. Cell* **8**, 305-320.
Locascio, A. and Nieto, M. A. (2001). Cell movements during vertebrate development: integrated tissue behaviour versus individual cell migration. *Curr. Opin. Genet. Dev.* **11**, 464-449.
Loosli, F., Winkler, S., Burgtorf, C., Wurmbach, E., Ansorge, W., Henrich, T., Grabher, C., Arendt, D., Carl, M., Krone, A. et al. (2001). Medaka *eyeless* is the key factor linking retinal dertermination and eye growth. *Development* **128**, 4035-4044.
Loosli, F., Del Bene, F., Quiring, R., Rembold, M., Martinez-Morales, J. R., Carl, M., Grabher, C., Iquel, C., Krone, A., Wittbrodt, B. et al. (2004). Mutations affecting retina development in Medaka. *Mech. Dev.* **121**, 703-714.

Lowery, L. A. and Sive, H. (2004). Strategies of vertebrate neurulation and a re-evaluation of teleost neural tube formation. *Mech. Dev.* **121**, 1189-1197.
Malicki, J. (2004). Cell fate decisions and patterning in the vertebrate retina: the importance of timing, asymmetry, polarity and waves. *Curr. Opin. Neurobiol.* **14**, 15-21.
Maniotis, A. J., Chen, C. S. and Ingber, D. E. (1997). Demonstration of mechanical connections between integrins, cytoskeletal filaments, and nucleoplasm that stabilize nuclear structure. *Proc. Natl. Acad. Sci. USA* **94**, 849-854.
Martin-Bermudo, M. D. and Brown, N. H. (1999). Uncoupling integrin adhesion and signaling: the betaPS cytoplasmic domain is sufficient to regulate gene expression in the Drosophila embryo. *Genes Dev.* **13**, 729-739.
Martinez-Morales, J. R., Naruse, K., Mitani, H., Shima, A. and Wittbrodt, J. (2004a). Rapid chromosomal assignment of Medaka mutants by bulked segregant analysis. *Gene* **329**, 159-165.
Martinez-Morales, J. R., Rodrigo, I. and Bovolenta, P. (2004b). Eye development: a view from the retina pigmented epithelium. *BioEssays* **26**, 766-777.
Martinez-Morales, J. R., Del Bene, F., Nica, G., Hammerschmidt, M., Bovolenta, P. and Wittbrodt, J. (2005). Differentiation of the vertebrate retina is coordinated by an FGF signaling center. *Dev. Cell* **8**, 565-574.
Morcillo, J., Martinez-Morales, J. R., Trousse, F., Fermin, Y., Sowden, J. C. and Bovolenta, P. (2006). Proper patterning of the optic fissure requires the sequential activity of BMP7 and SHH. *Development* **133**, 3179-3190.
Muyrers, J. P., Zhang, Y., Testa, G. and Stewart, A. F. (1999). Rapid modification of bacterial artificial chromosomes by ET-recombination. *Nucleic Acids Res.* **27**, 1555-1557.
Naruse, K., Fukamachi, S., Mitani, H., Kondo, M., Matsuoka, T., Kondo, S., Hanamura, N., Morita, Y., Hasegawa, K., Nishigaki, R. et al. (2000). A detailed linkage map of medaka, *Oryzias latipes*: comparative genomics and genome evolution. *Genetics* **154**, 1773-1784.
Nelson, W. J. (2003). Adaptation of core mechanisms to generate cell polarity. *Nature* **422**, 766-774.
Palmer, C. G., Bader, P., Slovak, M. L., Comings, D. E. and Pettenati, M. J. (1991). Partial deletion of chromosome 6p: delineation of the syndrome. *Am. J. Med. Genet.* **39**, 155-160.
Peters, M. A. (2002). Patterning the neural retina. *Curr. Opin. Neurobiol.* **12**, 43-48.
Pilot, F. and Lecuit, T. (2005). Compartmentalized morphogenesis in epithelia: from cell to tissue shape. *Dev. Dyn.* **232**, 685-694.
Rembold, M., Loosli, F., Adams, R. J. and Wittbrodt, J. (2006). Individual cell migration serves as the driving force for optic vesicle evagination. *Science* **313**, 1130-1134.
Retta, S. F., Balzac, F., Ferraris, P., Belkin, A. M., Fassler, R., Humphries, M. J., De Leo, G., Silengo, L. and Tarone, G. (1998). beta1-integrin cytoplasmic subdomains involved in dominant negative function. *Mol. Biol. Cell* **9**, 715-731.
Schmitt, E. A. and Dowling, J. E. (1994). Early eye morphogenesis in the zebrafish, Brachydanio rerio. *J. Comp. Neurol.* **344**, 532-542.
Schock, F. and Perrimon, N. (2002). Molecular mechanisms of epithelial morphogenesis. *Annu. Rev. Cell Dev. Biol.* **18**, 463-493.
Spemann, H. (1901). Über die Korrelation der Entwicklung des Auges. *Verh. Anat. Ges.* **15**, 61-79.
Thermes, V., Grabher, C., Ristoratore, F., Bourrat, F., Choulika, A., Wittbrodt, J. and Joly, J. S. (2002). I-SceI meganuclease mediates highly efficient transgenesis in fish. *Mech. Dev.* **118**, 91-98.
Torres, M., Gómez-Pardo, E. and Gruss, P. (1996). *Pax2* contributes to inner ear patterning and optic nerve trajectory. *Development* **122**, 3381-3391.
Turner, C. E. (2000). Paxillin and focal adhesion signalling. *Nat. Cell Biol.* **2**, E231-E236.
von Trotha, J. W., Campos-Ortega, J. A. and Reugels, A. M. (2006). Apical localization of ASIP/PAR-3:EGFP in zebrafish neuroepithelial cells involves the oligomerization domain CR1, the PDZ domains, and the C-terminal portion of the protein. *Dev. Dyn.* **235**, 967-977.
Wallingford, J. B. (2005). Neural tube closure and neural tube defects: studies in animal models reveal known knowns and known unknowns. *Am. J. Med. Genet. C Semin. Med. Genet.* **135**, 59-68.
West, K. A., Zhang, H., Brown, M. C., Nikolopoulos, S. N., Riedy, M. C., Horwitz, A. F. and Turner, C. E. (2001). The LD4 motif of paxillin regulates cell spreading and motility through an interaction with paxillin kinase linker (PKL). *J. Cell Biol.* **154**, 161-176.
Young, P. E., Pesacreta, T. C. and Kiehart, D. P. (1991). Dynamic changes in the distribution of cytoplasmic myosin during Drosophila embryogenesis. *Development* **111**, 1-14.